Applied Catalysis B: Environmental 243 (2019) 212–219

Contents lists available at ScienceDirect

Applied Catalysis B: Environmental

journal homepage: www.elsevier.com/locate/apcatb

Economical synthesis of high-silica LTA zeolites: A step forward in developing a new commercial NH_3-SCR catalyst

Donghui Jo[1], Gi Tae Park[1], Taekyung Ryu, Suk Bong Hong*

Center for Ordered Nanoporous Materials Synthesis, Division of Environmental Science and Engineering, POSTECH, Pohang 37673, Republic of Korea

ARTICLE INFO

Keywords:
Cu-LTA
Economical synthesis
Characterization
NH_3-SCR
Hydrothermal stability

ABSTRACT

Here we report an economical synthesis method for high-silica (Si/Al ~ 17) LTA zeolites using colloidal silica and ammonium fluoride as Si and F sources, respectively. When both 1,2-dimethyl-3-(4-methylbenzyl)imidazolium and tetramethylammonium ions are used as organic structure-directing agents, the LTA crystallization was found to strongly depend on the particle size of the colloidal silica employed. However, the type of Al and F sources had little effect on the formation of this small-pore zeolite. The catalytic properties of three high-silica Cu-LTA catalysts synthesized using the same Si source (Ludox HS-40 colloidal silica) but different Al sources (aluminum hydroxide, aluminum metal, and pseudoboehmite) for the selective catalytic reduction of NO_x with NH_3 (NH_3-SCR) are also presented. Despite the presence of a large amount of extraframework Al, all of the catalysts exhibited considerably higher activity maintenance than the current commercial Cu-SSZ-13 catalyst even after hydrothermal aging at 900 °C.

1. Introduction

As the regulation standards on nitrogen oxides (NO_x) emission from motor vehicles are becoming tighter, selective catalytic reduction of NO_x with urea and thus with ammonia (NH_3-SCR), a technology to facilitate NO_x removal in oxygen-rich exhaust from fuel-efficient diesel engines, has received much attention in the automobile industry [1–3]. While various metal-exchanged zeolites have been intensively evaluated as NH_3-SCR diesel vehicle catalysts over the past several decades, copper-exchanged SSZ-13 (framework type CHA) is the current commercial choice, because of its excellent hydrothermal stability [4–11]. However, there is a need for the catalyst to be closer to the diesel particulate filter, which must be periodically regenerated at high temperatures prior to a certain level of soot accumulation [12]. Owing to the resulting large temperature spikes, therefore, the development of catalysts with better hydrothermal stability is still of major importance in mobile SCR technology [13–15].

Zeolite A (LTA) is the most symbolic among the zeolites known to date in that it is the first synthetic zeolite to be prepared [16], whereas its natural counterpart has not been discovered yet. This cage-based small-pore zeolite has a high Al content (Si/Al = 1.0) and thus a poor stability. However, the recent success of the synthesis of high-silica (Si/Al > 8) LTA zeolites using both 1,2-dimethyl-3-(4-methylbenzyl) imidazolium and tetramethylammonium ions as organic structure-directing agents (OSDAs) in fluoride media [17,18] has provided a new impetus for zeolite catalysis. Importantly, fully copper-exchanged (Cu/Al ~ 0.50) high-silica (Si/Al = 16-23) LTA zeolites exhibit remarkable NH_3-SCR activity even after hydrothermal aging at 900 °C, the temperature at which the current commercial Cu-SSZ-13 catalyst loses its structural integrity and activity, opening up a new direction for the development of advanced SCR catalysts [19,20].

From economic, safety, health, and/or environmental points of view, on the other hand, the reagents normally used in laboratory zeolite synthesis, are not often suitable for industrial-scale production [21,22]. For example, tetraethylorthosilicate is not a commercially viable Si source, because of its expensive cost, as well as the large amounts of ethanol and heat released during hydrolysis. Also, hydrofluoric acid, which is a solution of hydrogen fluoride (HF) in water and is commonly used as a F source in fluoride-mediated zeolite synthesis, cannot be a proper reagent in a practical manufacturing process due to its high corrosiveness and toxicity. Unfortunately, these two raw materials were originally used in the benzylimidazolium-mediated synthesis of high-silica LTA zeolites [17,18], restricting their commercial use as an NH_3-SCR catalyst support.

In the present study we describe our attempts to develop an industrially friendly synthesis route to high-silica LTA zeolites using

* Corresponding author.
E-mail address: sbhong@postech.ac.kr (S.B. Hong).
[1] These authors contributed equally to this work.

https://doi.org/10.1016/j.apcatb.2018.10.042
Received 26 June 2018; Received in revised form 13 October 2018; Accepted 17 October 2018
Available online 22 October 2018
0926-3373/

economical and less hazardous Si and F sources. We also report the NH_3-SCR performance of the copper-exchanged form of LTA zeolites synthesized in this way. The catalytic results are compared with those obtained from Cu-LTA with similar Cu/Al and Si/Al ratios prepared by the original synthesis procedure [18], as well as from Cu-SSZ-13. Changes in the physicochemical properties of the economically synthesized Cu-LTA catalysts caused by hydrothermal aging at high temperatures have been extensively characterized by using powder X-ray diffraction, N_2 adsorption, NH_3 temperature-programmed desorption, and ^{27}Al MAS NMR, IR, UV-vis, and Cu K-edge X-ray absorption near edge structure spectroscopies.

2. Experimental

2.1. Zeolite synthesis

The reagents employed included 1,2-dimethyl-3-(4-methylbenzyl) imidazolium (12DM3(4MB)I) hydroxide, tetramethylammonium hydroxide pentahydrate (TMAOH·5H_2O, 97%, Aldrich), hydrofluoric acid (HF, 48%, J.T. Baker), ammonium fluoride (NH_4F, 98%, Aldrich), aluminum hydroxide ($Al(OH)_3$·H_2O, Aldrich), aluminum metal (99.5%, Alfa), pseudoboehmite (Catapal B, Vista), three colloidal silicas with different average particle sizes (Ludox AS-40, 22 nm, 40%; Ludox HS-40, 12 nm, 40%; Ludox SM, 7 nm, 30%; all from Aldrich), fumed silica (Aerosil 200, Degussa), and tetraethylorthosilicate (TEOS, 98%, Aldrich). 12DM3(4MB)I hydroxide was synthesized according to the procedure in the literature [18]. The composition of the final synthesis mixture was 0.5ROH·xTMAOH·0.50AF·1.0SiO_2·0.5xAl_2O_3·5.0H_2O, where R is 12DM3(4MB)I, x is varied between 0 and 0.133, and A is H or NH_4, unless otherwise stated. A small amount (4 wt% of the silica in the synthesis mixture) of calcined LTA with Si/Al = 23 was added as seed crystals to the final synthesis mixture and stirred for 24 h, unless otherwise stated. The final synthesis mixture was charged into Teflon-lined 23 mL autoclaves and heated under rotation (60 rpm) at 175 °C for the desired time.

As-made LTA zeolites were calcined in air at 600 °C for 8 h to remove the occluded OSDA molecules. The calcined samples were converted into the ammonium form by refluxing twice in 1.0 M NH_4NO_3 solutions (2.0 g solid per 100 mL solution) for 6 h. For comparison, SSZ-13 (Si/Al = 16) was synthesized following the procedure described elsewhere [23]. Copper-exchanged zeolites employed here were prepared by ion exchange of their ammonium form using 0.01 M $Cu(CH_3COO)_2$ (97%, Aldrich) solutions at room temperature, where the number and time of ion exchange were properly adjusted to obtain fully copper-exchanged (Cu/Al ~ 0.50) catalysts, dried at 90 °C overnight, and calcined in air at 550 °C for 8 h prior to the use as catalysts. The catalysts were aged under flowing air containing 10% H_2O at 750, 850, and 900 °C for up to 24 h in order to examine their hydrothermal stability.

2.2. Catalysis

The deNO_x activity test was conducted under atmospheric pressure in a fixed-bed flow reactor (3/8-in.-od Al tube) [9]. Prior to each experiment, 0.6 g of catalyst (20/30 mesh size) packed into the reactor were heated from room temperature to 500 °C at a heating rate of 10 °C min^{-1} under 21% O_2/N_2 flow (2000 mL min^{-1}) and held at the final temperature for 2 h. A feed gas composition containing 500 ppm NH_3, 500 ppm NO, 5% O_2, 10% H_2O, and N_2 was supplied through mass flow controllers, and the gas hourly space velocity (GHSV) was maintained at 100,000 h^{-1}. The inlet and outlet concentrations of NO were determined by an online Nicolet 6700 FT-IR spectrometer equipped with a 2 m gas cell.

2.3. Analytical methods

The powder X-ray diffraction (XRD) patterns were measured on a PANalytical X'Pert diffractometer (Cu Kα radiation) with an X'Celerator detector. The relative crystallinities of a series of solid products recovered at different time intervals were determined by comparing the height of the intense X-ray peak around 2θ = 22.4°, corresponding to the (622) reflection of the LTA structure, with that of a fully crystallized sample. Elemental analysis for Si, Al, and Cu was performed by the analytical laboratory of the Pohang Institute of Metal Industry Advancement. Crystal morphology and average size were determined by a JEOL JSM-6510 scanning electron microscope (SEM). N_2 sorption experiments were carried out on a Mirae SI Nanoporosity-XQ analyzer. NH_3 temperature-programmed desorption (NH_3 TPD) was performed on a fixed bed, flow-type apparatus linked to a Hewlett-Packard 5890 series II gas chromatograph with a thermal conductivity detector, according to the procedures given in our previous work [15].

The ^{27}Al MAS NMR spectra were measured on a Bruker DRX500 spectrometer at a ^{27}Al frequency of 130.318 MHz and a spinning rate of 21 kHz with a $\pi/6$ rad pulse length of 2.0 μs, a recycle delay of 0.5 s, and an acquisition of ca. 1000 pulse transients. The ^{27}Al chemical shifts are referenced to an $Al(H_2O)_6^{3+}$ solution. The IR spectra in the OH region were recorded on a Nicolet 6700 FT-IR spectrometer using self-supporting zeolite wafers of ca. 13 mg cm^{-2}. Prior to IR measurements, the zeolite wafers were activated under vacuum (10^{-4} Pa) at 450 °C for 2 h inside a home-built IR cell with CaF_2 windows. When using NH_3 as a probe molecule to investigate the acidic properties of LTA zeolites, the activated self-supporting wafer was contacted with a dry He flow containing ammonia of 1.3 × 10^3 Pa at 150 °C for 0.5 h and evacuated (10^{-4} Pa) at the same temperature for 0.5 h to remove physisorbed NH_3 and then heated at temperatures up to 350 °C. The concentrations of Brønsted and Lewis acid sites were determined from the intensities of the IR bands around 1455 and 1620 cm^{-1}, respectively, by using the extinction coefficients (12.48 ± 0.5 cm $mmol^{-1}$ for Brønsted acid sites and 0.28 ± 0.1 cm $mmol^{-1}$ for Lewis acid sites) obtained using the method of Wichterlová et al. [24].

The UV–vis spectra were recorded on a Shimadzu UV-2501PC spectrometer in diffuse reflectance mode between 200 and 800 nm at a step of 0.5 nm with a slit width of 1.0 nm, using $BaSO_4$ as a reference. The X-ray absorption near edge structure (XANES) spectra at the Cu K-edge were collected on the 8C beamline at the Pohang Accelerator Laboratory (PAL) using a Si (111) crystal monochromator. Cu foil was employed for the energy calibration (E_0 = 8979.0 eV). The X-ray intensity was monitored using ionization chambers purged with pure N_2 gas at room temperature for the incident (I_0) and transmitted (I_t) beam in the Cu K-edge measurements. Cu_2O (≥99.99%, Aldrich) and CuO (99.99%, Aldrich) were used as reference compounds.

3. Results and discussion

3.1. Synthesis

Table 1 lists the results from syntheses using 12DM3(4MB)I and TMA ions as OSDAs and a series of synthesis mixtures with the same Si/Al ratio (15) but made up of different raw material sources under the conditions described above. We selected this particular Si/Al ratio for LTA synthesis because, even after hydrothermal aging at 900 °C, Cu-LTA zeolites with such a Si/Al ratio showed excellent NH_3-SCR activity [19]. The solid products listed in Table 1 were the only ones obtained in repeated trials.

It can be seen that the use of only half of the HF content in the original synthesis recipe for an LTA zeolite with Si/Al = 16 [18] resulted in the formation of a considerable amount of RUT zeolite as an impurity phase. This suggests that the presence of a certain F^- ion concentration is required for LTA crystallization. Our initial attempts to economically synthesize LTA zeolites were made to replace TEOS with other inexpensive Si sources while keeping HF as a F source. The use of Aerosil 200 fumed silica under the conditions, where the LTA crystallization by means of TEOS proved to be highly reproducible, gave no crystalline phase even after 7 days of heating at 175 °C. When heating

Table 1
LTA zeolite syntheses using aluminosilicate mixtures with the same Si/Al ratio (15) but made up of different raw material sources.[a]

Run	Si source[b]	Al source[c]	F source	Product	Si/Al in the product	Sample ID[d]
1[e]	TEOS	AH	HF	LTA	16	LTA(O)
2[f]	TEOS	AH	HF	LTA + RUT		
3[g]	Aerosil 200	AH	HF	Amorphous		
4[h]	Ludox AS-40 (22)	AH	HF	Amorphous		
5	Ludox HS-40 (12)	AH	HF	LTA		
6	Ludox HS-40 (12)	AH	NH_4F	LTA	16	LTA(E)AH
7	Ludox HS-40 (12)	AM	NH_4F	LTA	17	LTA(E)AM
8	Ludox HS-40 (12)	PB	NH_4F	LTA	18	LTA(E)PB
9	Ludox SM (7)	AH	HF	LTA		
10	Ludox SM (7)	AH	NH_4F	LTA		

[a] The composition of the synthesis mixture is $0.5ROH{\cdot}0.067TMAOH{\cdot}0.50AF{\cdot}1.0SiO_2{\cdot}0.033Al_2O_3{\cdot}5.0H_2O$, where R is 12DM3(4MB)I and A is H or NH_4. A small amount (4 wt% of the silica in the synthesis mixture) of calcined LTA with Si/Al = 23 was added as seed crystals to the synthesis mixture. The crystallization was performed under rotation (60 rpm) at 175 °C for 1 day, unless otherwise stated.
[b] The values in parentheses are the manufacturer-specified average particle diameter in nm of colloidal silica.
[c] AH, aluminum hydroxide; AM, aluminum metal; PB, pseudobohemite.
[d] The letters O and E in parentheses of the sample ID designate that the zeolite was synthesized using the original and economical ways, respectively, and its suffix letters represent the Al source employed.
[e] Run performed according to the original recipe in Ref. [18].
[f] Run performed using the half amount of HF in the original recipe. The product appearing first is the major phase.
[g] Run performed for 7 days.
[h] Run performed for 3 days.

for 14 days, in addition, we obtained only an MTN-type material (Supplementary Table S1). This led us to focus on the utilization of colloidal silica as a Si source. The replacement of TEOS with Ludox AS-40 colloidal silica yielded an amorphous product after 3 days of heating. Also, an additional 4 days of heating resulted in the cocrystallization of MTN and RUT zeolites, where the former material was the major phase (Supplementary Table S1).

As shown in Table 1, however, the use of Ludox HS-40 with a smaller average diameter (12 vs 22 nm) directed the synthesis of LTA zeolites after 1 day. The same result was obtained when Ludox SM with an average diameter of 7 nm was used as a Si source. It thus appears that the average particle size of colloidal silica is a crucial factor governing the crystallization of LTA zeolites. Considering that the Na content (Na/Si = 0.016) of Ludox AS-40 is smaller than that (Na/Si = 0.020-0.039) of Ludox HS-40 and Ludox SM, the presence of a small amount of Na in the synthesis mixture does not seem to hinder LTA formation. Table 1 also shows that LTA crystallization is possible by the combined use of NH_4F, a safer F source in handling than HF, and Ludox HS-40. Furthermore, when Ludox HS-40 and NH_4F were fixed as Si and F sources, respectively, the replacement of aluminum hydroxide with Al metal or pseudoboehmite gave pure LTA after 1 day of heating at 175 °C. These results indicate that LTA crystallization is not strongly influenced by the type of both Al and F sources, unlike the case of the Si source. It is worth noting that this cage-based small-pore zeolite can be synthesized over a wide Si/Al ratio range (7.5-∞) using Ludox HS-40 and NH_4F (Supplementary Table S1).

Fig. 1 shows the crystallization kinetics of the four LTA zeolites obtained using aluminosilicate mixtures with the same synthesis mixture composition (12DM3(4MB)I/TMA = 7.5 and Si/Al = 15) but different Si, Al, and/or F sources at 175 °C under rotation (60 rpm). As shown in Table 1, these zeolites are characterized by quite similar bulk Si/Al ratios (16–18) to one another, but were synthesized either following the original recipe, which includes the use of TEOS, aluminum hydroxide, and HF [18], or using three different Al sources (i.e., aluminum hydroxide (AH), aluminum metal (AM), and pseudoboehmite (PB)) in the presence of Ludox HS-40 and NH_4F as Si and F sources, respectively. From now on, we will refer to them as LTA(O), LTA(E)AH, LTA(E)AM, and LTA(E)PB, where the letters O and E in parentheses designate that the zeolite has been synthesized using the original and economical ways, respectively. Also, the suffix letters represent the Al source employed.

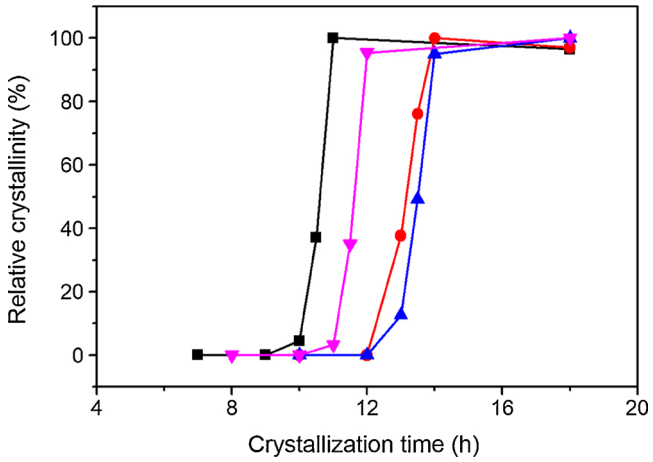

Fig. 1. Crystallinities of LTA(O) (■), LTA(E)AH (●), LTA(E)AM (▲), and LTA(E)PB (▼) as a function of crystallization time from the same synthesis mixture composition (12DM3(4MB)I/TMA = 7.5 and Si/Al = 15; Table 1) at 175 °C under rotation (60 rpm).

The synthesis results in Fig. 1 and Supplementary Fig. S1 reveal that all the LTA zeolites began to rapidly grow after some induction period. Also, although LTA(O) crystallization showed a shorter induction period compared to the other three cases, differences (< 4 h) in the induction period were not so large. Thus, these four LTA zeolites fully crystallized after ca. 10–14 h of heating, which has an advantage from the viewpoint of mass production. It should be noted that all of them are stable for an additional one week of heating in the crystallization medium. Their powder XRD patterns and SEM images are shown in Fig. 2. Each LTA zeolite is highly crystalline and phase-pure, which can be further supported by the N_2 BET surface areas in Table 2. Also, no significant differences in the crystal morphology and size were found.

3.2. Catalytic performance

Fig. 3 shows NO conversion as a function of temperature in the NH_3-SCR reaction over the fresh, 750 °C-, 850 °C-, and 900 °C-aged forms of Cu-LTA(O), Cu-LTA(E)AH, Cu-LTA(E)AM, Cu-LTA(E)PB, and Cu-SSZ-13 catalysts measured at 500 ppm NH_3, 500 ppm NO, 5% O_2, and 10% H_2O

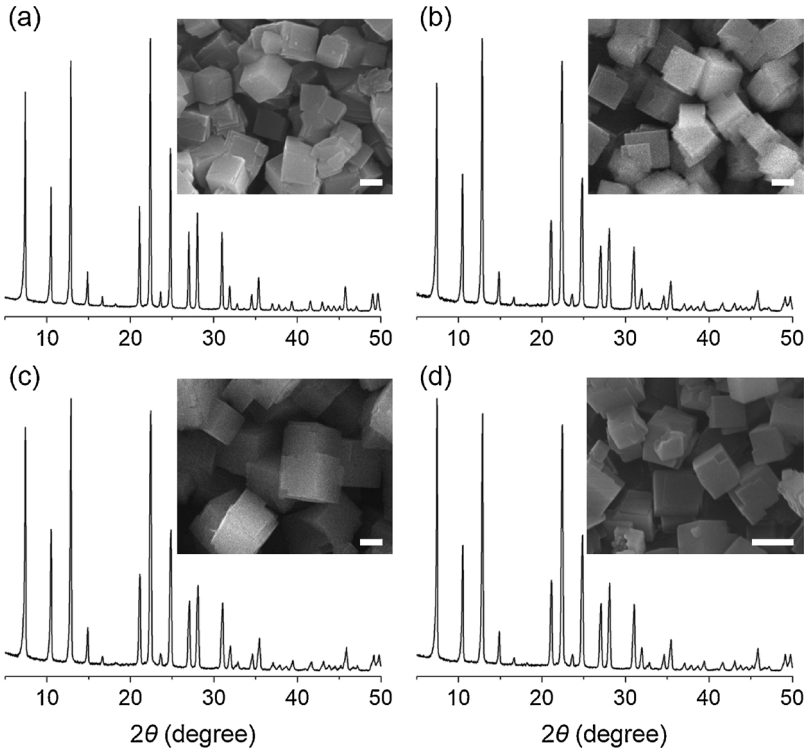

Fig. 2. Powder XRD patterns and SEM images (scale bar, 1 μm) of as-made (a) LTA(O), (b) LTA(E)AH, (c) LTA(E)AM, and (d) LTA(E)PB.

Table 2
Physicochemical properties of Cu^{2+}-exchanged zeolite catalysts prepared in this study.

Catalyst ID	Si/Al[a]	Crystal shape and size[b] (μm)	Cu[a] (wt%)	Cu/Al[a]	BET surface area[c,d] ($m^2\,g^{-1}$)		
					Total	Microporous	External
Cu-LTA(O)	16	cubes, 1.7	2.7	0.48	670 (740)	600 (660)	70 (80)
Cu-LTA(E)AH	16	cubes, 1.6	2.5	0.46	685 (760)	620 (680)	65 (80)
Cu-LTA(E)AM	17	cubes, 2.1	2.4	0.46	690 (750)	610 (655)	80 (95)
Cu-LTA(E)PB	18	cubes, 1.1	2.4	0.50	645 (755)	580 (675)	65 (80)
Cu-SSZ-13	16	ellipsoids, 1.1 × 1.5	2.8	0.49	520 (725)	475 (665)	45 (60)

[a] Determined by elemental analysis.
[b] Determined by SEM.
[c] Calculated from N_2 adsorption data.
[d] The values in parentheses are the surface area of the proton form of each catalyst.

in the feed and at 100,000 h^{-1} GHSV. Because the Cu/Al (0.48 ± 0.02) and Si/Al (17 ± 1) ratios of the four Cu-LTA catalysts are essentially identical to one another (Table 2), the catalytic results in Fig. 3 will reveal differences in the intrinsic properties of the respective LTA zeolite supports. When fresh, no noticeable differences in the low-temperature SCR activity were observed between Cu-LTA(O) and the other three Cu-LTA catalysts whose zeolite supports were synthesized using more economical and safer reagents (Table 1). These almost fully copper-exchanged LTA catalysts are slightly less active in the low-temperature region than Cu-SSZ-13. However, the opposite was observed for the NO conversion at 450 °C or higher.

Fig. 3 also shows that even after hydrothermal aging at 750 or 850 °C for 24 h, Cu-LTA(E)AH, Cu-LTA(E)AM, and Cu-LTA(E)PB, as well as Cu-LTA(O), maintain their deNO_x activity in the temperature range studied here, validating their outstanding hydrothermal durability. However, as recently demonstrated by us [19], Cu-SSZ-13 lost its high-temperature activity after hydrothermal aging at 750 °C and became completely deactivated after aging at 850 °C. Unlike the other three Cu-LTA catalysts, on the other hand, Cu-LTA(E)PB when hydrothermally aged at 900 °C for 12 h exhibited a rapid decrease in high-temperature deNO_x activity. These results clearly show that the synthesis of hydrothermally stable LTA zeolites can be achieved in an economical way, but their relative stability can differ according to the type of raw material sources employed, particularly the Al source.

3.3. Characterization

The powder XRD patterns of fresh Cu-LTA(O), Cu-LTA(E)AH, Cu-LTA(E)AM, and Cu-LTA(E)PB zeolites and their hydrothermally aged form at different temperatures can be found in Supplementary Fig. S2. None of these catalysts showed a notable decrease in XRD peak intensity even after aging at 900 °C. Since there are no X-ray reflections assignable to copper oxide species, in addition, the size of copper oxide particles, if generated during calcination and/or hydrothermal aging, may be too small to be detected by powder XRD. By contrast, Cu-SSZ-13 was found to be become amorphous during aging at 850 or 900 °C (Supplementary Fig. S3), explaining its catalytic behavior in Fig. 3. Changes in the N_2 BET surface area of these four Cu-LTA zeolites caused by hydrothermal aging at temperatures up to 900 °C are compared in Fig. 4. No detectable decrease in BET surface area was observed for Cu-

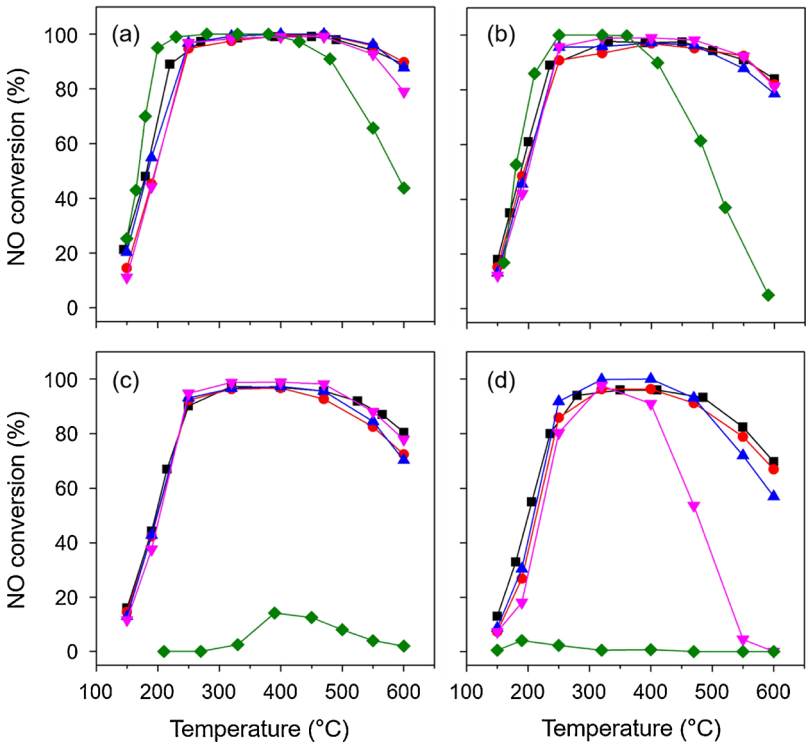

Fig. 3. NO conversion as a function of temperature in NH_3-SCR reaction over the (a) fresh, (b) 750 °C-, (c) 850 °C-, and (d) 900 °C-aged forms of Cu-LTA(O) (■), Cu-LTA(E)AH (●), Cu-LTA(E)AM (▲), Cu-LTA(E)PB (▼), and Cu-SSZ-13 (◆) catalysts. The feed contains 500 ppm NH_3, 500 ppm NO, 5% O_2, 10% H_2O balanced with N_2 at 100,000 h^{-1} GHSV. Hydrothermal aging was performed under flowing air containing 10% H_2O at 750 and 850 °C for 24 h and at 900 °C for 12 h.

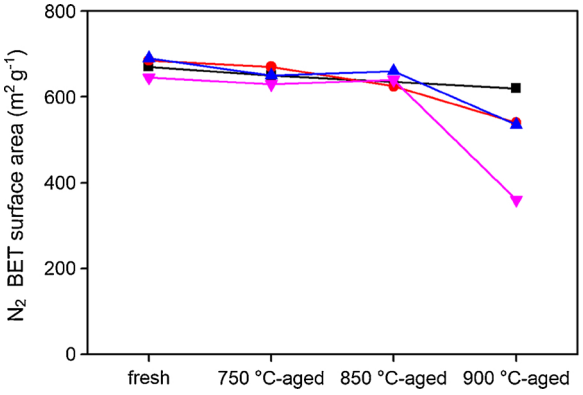

Fig. 4. N_2 BET surface areas of Cu-LTA(O) (■), Cu-LTA(E)AH (●), Cu-LTA(E)AM (▲), and Cu-LTA(E)PB (▼) hydrothermally aged at different temperatures. The hydrothermal aging conditions are the same as those in Fig. 3.

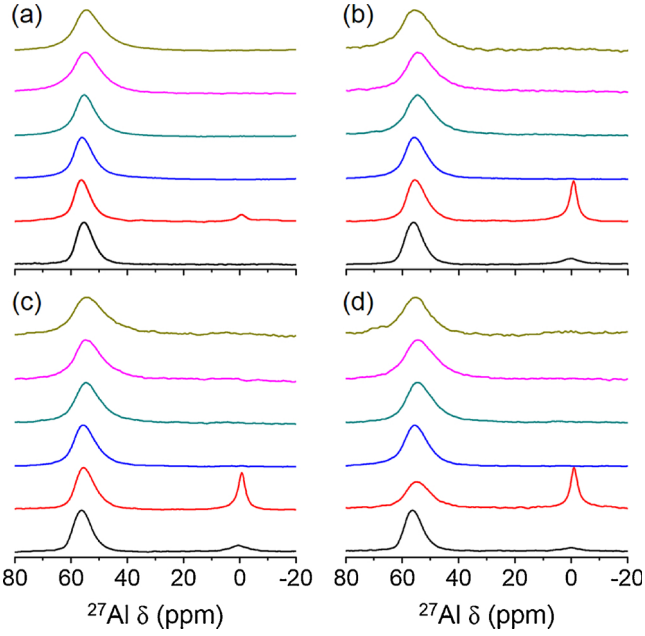

Fig. 5. ^{27}Al MAS NMR spectra of the (from bottom to top) as-made, proton, and copper-exchanged forms of (a) LTA(O), (b) LTA(E)AH, (c) LTA(E)AM, and (d) LTA(E)PB. The spectra of Cu-LTA zeolites are given in the order of fresh, 750 °C-, 850 °C-, and 900 °C-aged ones, from bottom to top. The hydrothermal aging conditions are the same as those in Fig. 3.

LTA(O), Cu-LTA(E)AH, and Cu-LTA(E)AM. However, although the surface area of fresh Cu-LTA(E)PB is essentially the same as that of the 850 °C-aged one, it decreased by nearly half with aging at 900 °C, indicating that the zeolite support structure has been severely damaged. This may explain why 900 °C-aged Cu-LTA(E)PB displays a sharp drop in high-temperature deNO_x activity (Fig. 3).

Fig. 5 shows the ^{27}Al MAS NMR spectra of the as-made and proton forms of LTA(O), LTA(E)AH, LTA(E)AM, and LTA(E)PB, as well as their copper-exchanged forms before and after hydrothermal aging at different temperatures. Unlike the spectrum of as-made LTA(O) characterized by only one ^{27}Al resonance around 56 ppm, typical of tetrahedral Al, the spectra of the other three as-made LTA zeolites synthesized in an economical way gave an additional weak signal around 0 ppm due to extraframework octahedral Al. If the homogeneity of the synthesis mixture is a key factor in obtaining extraframework Al-free LTA crystals, then the use of monomeric TEOS as a Si source, rather than of polymeric colloidal silica particles, would be more favorable. Also, all the spectra of the proton forms showed a much stronger ^{27}Al resonance around 0 ppm compared to the spectrum of H-LTA(O), suggesting that the thermal stability of Al in the LTA framework differs according to the type of Si and/or F sources employed.

Due to the stronger interactions of paramagnetic Cu^{2+} ions with octahedral Al species than with framework Al atoms, on the other hand, there are no detectable signals around 0 ppm in the ^{27}Al MAS NMR spectra of not only fresh Cu-LTA zeolites but also their hydrothermally aged form, regardless of the aging temperature. Nevertheless, it is not difficult to conjecture that the concentration of extraframework Al

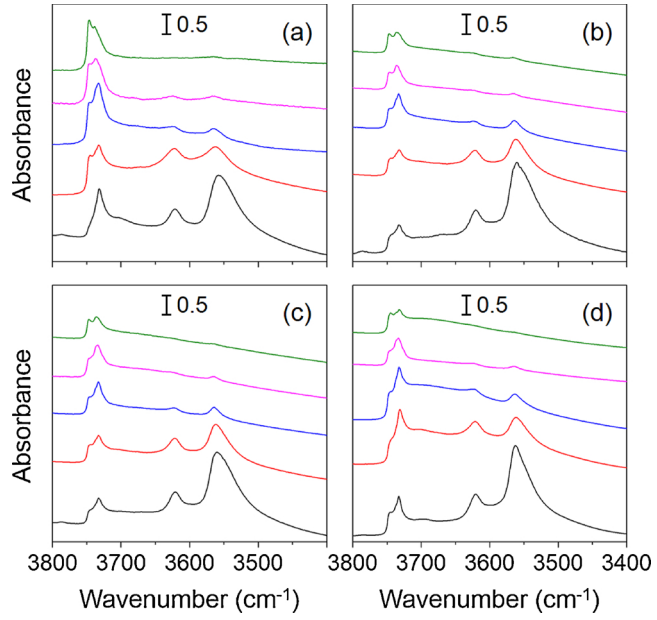

Fig. 6. IR spectra in the OH stretching region of the proton and copper-exchanged forms of LTA(O), (b) LTA(E)AH, (c) LTA(E)AM, and (d) LTA(E)PB. The spectra of the latter form are given in the order of fresh, 750 °C-, 850 °C-, and 900 °C-aged Cu-LTA zeolites (from second bottom to top). The hydrothermal aging conditions are the same as those in Fig. 3.

species may be fairly lower in Cu-LTA(O) than in the other three Cu-LTA zeolites. As shown in Fig. 3, the deNO$_x$ activity of 900 °C-aged Cu-LTA(E)AH and Cu-LTA(E)AM is quite similar to that of 900 °C-aged Cu-LTA(O), implying that zeolite extraframework Al species do not play a role in NH$_3$-SCR. We note that, when aged at 850 or 900 °C, the ^{27}Al MAS NMR spectrum of Cu-SSZ-13 is characterized by a very broad resonance around 40 ppm (Supplementary Fig. S4), in good agreement with the powder XRD results in Supplementary Fig. S3.

Fig. 6 shows the IR spectra in the OH stretching region of H-LTA(O), H-LTA(E)AH, H-LTA(E)AM, and H-LTA(E)PB and their copper-exchanged zeolites before and after hydrothermal aging at different temperatures. All the spectra of the proton form of these four LTA zeolites are characterized by two well-resolved IR bands around 3620 and 3550 cm^{-1} assignable to the bridging Si-OH-Al groups pointed into the large *lta* cages and in the 6-ring windows of the considerably smaller *sod* cages, respectively [25]. IR analysis of preadsorbed NH$_3$ indicates that the number of Brønsted acid sites is larger in H-LTA(O) than in the other H-LTA zeolites (Supplementary Table S2), which is in good agreement with the ^{27}Al MAS NMR results in Fig. 5. However, since the opposite is the case for Lewis acid sites, the total numbers (0.43-0.45 mmol NH$_3$ g^{-1}) of acidic sites in these four H-LTA zeolites were found to be quite similar to one another. The IR spectra of fresh Cu-LTA(O), Cu-LTA(E)AH, Cu-LTA(E)AM, and Cu-LTA(E)PB zeolites also show two bridging OH bands. As shown in Fig. 6, however, the intensities of both OH bands are fairly weak compared to those observed for the proton form of the corresponding LTA zeolites. Moreover, these two bands become hardly detectable with increasing hydrothermal aging temperature to 900 °C, probably due to the additional dealumination that should be more severe at a higher temperature.

Fig. 7 compares the NH$_3$ TPD profiles of H-LTA(O), H-LTA(E)AH, H-LTA(E)AM, and H-LTA(E)PB with their copper-exchanged zeolites before and after hydrothermal aging at 900 °C. The TPD profiles of their proton forms show two desorption peaks with maxima at 250 and 390 °C assigned to NH$_3$ desorption from weak and strong acid sites, respectively. Also, the areas (i.e., the density of acid sites) of both peaks are quite similar for these four zeolites, which is in line with the NH$_3$ IR results in Supplementary Table S2. Essentially the same trend was observed for the profiles of the four fresh Cu-LTA zeolites. As shown in Fig. 7, however, the low-temperature and high-temperature desorption peaks are considerably stronger and weaker than those observed for the proton form of the corresponding zeolites, respectively. Therefore, the low-temperature peak appears to be assignable to NH$_3$ desorption from the Lewis acid sites generated by Cu^{2+} ion exchange. When correlated with the IR results in Fig. 6, in addition, the high-temperature peak can be mainly attributed to the Brønsted acid sites in zeolite supports. Fig. 7 also shows that after thermal aging at 900 °C, the high-temperature NH$_3$ desorption peak from each Cu-LTA zeolite becomes weaker again. Recall that there are no noticeable differences in the deNO$_x$ activity between the fresh and 900 °C-aged forms of Cu-LTA(E)AH, Cu-LTA(E)AM, and Cu-LTA(O) (Fig. 3). Therefore, it is most likely that the Brønsted acid sites in Cu-LTA zeolites have little effect on NH$_3$-SCR, as recently reported [19].

Fig. 8 shows the UV–vis spectra of the fresh and 900 °C-aged forms of four copper-exchanged LTA zeolites studied in this work. The spectra of all fresh catalysts give two broad bands around 240 and 780 nm attributable to the $O \rightarrow Cu^{2+}$ charge-transfer and the *d-d* transition of Cu^{2+} ($3d^9$) ions, respectively [26,27], indicating that the isolated Cu^{2+} ions are the most dominant copper species [8,10]. We note here that the charge-transfer band is red-shifted after hydrothermal aging at 900 °C, which may be a consequence of the conversion of exchanged copper ions to oligonuclear [Cu-O-Cu]$_n$ (280–330 nm) and crystalline CuO$_x$ (330–420 nm) species [26,27]. Among the 900 °C-aged catalysts, only Cu-LTA(E)PB exhibits a shoulder around 380 nm, suggesting a severer sintering of CuO$_x$ species in this catalyst. This is not unexpected given its relatively poor thermal stability (Fig. 4), and such copper species could be more active for NH$_3$ oxidation at high temperatures than for NH$_3$-SCR [28].

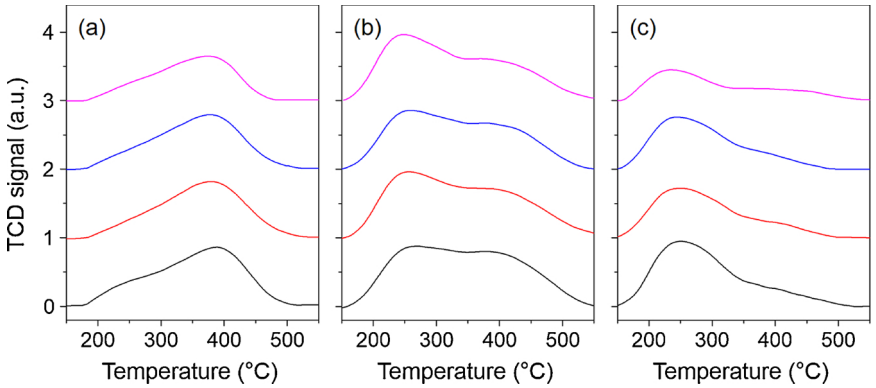

Fig. 7. NH$_3$ TPD profiles of the (a) proton, (b) fresh, copper-exchanged, and (c) 900 °C-aged, copper-exchanged forms of (from bottom to top) LTA(O), LTA(E)AH, LTA(E)AM, and LTA(E)PB.

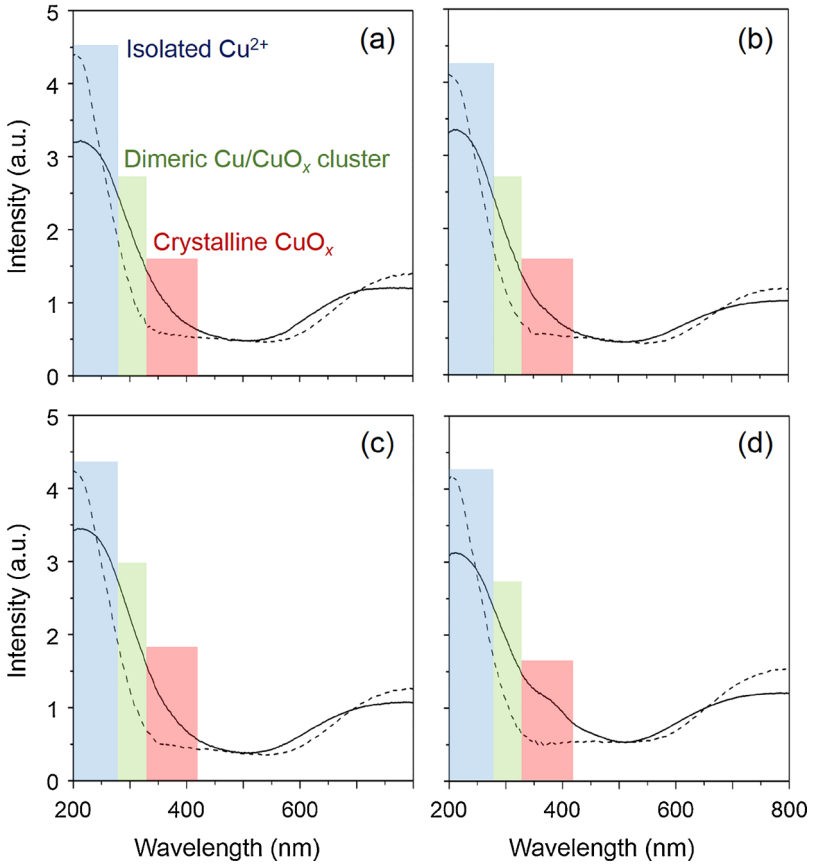

Fig. 8. UV–vis spectra of (a) Cu-LTA(O), (b) Cu-LTA(E)AH, (c) Cu-LTA(E)AM, and (d) Cu-LTA(E)PB before (dotted line) and after (solid line) hydrothermal aging at 900 °C for 12 h.

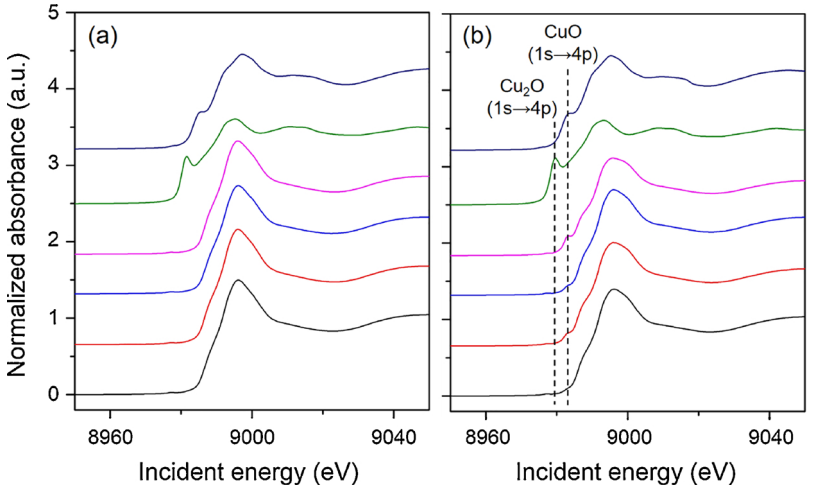

Fig. 9. Cu K-edge XANES spectra of (from bottom to top) Cu-LTA(O), Cu-LTA(E)AH, Cu-LTA(E)AH, Cu-LTA(E)PB, Cu_2O, and CuO before (left) and after (right) hydrothermal aging at 900 °C for 12 h.

Fig. 9 shows the Cu K-edge XANES spectra of Cu-LTA(O), Cu-LTA(E)AH, Cu-LTA(E)AM, and Cu-LTA(E)PB before and after hydrothermal aging at 900 °C. These data reveal that most of the copper species in fresh catalysts are present as divalent cations, which may also be the case for 900 °C-aged catalysts. However, the XANES spectra of some 900 °C-aged catalysts, particularly the spectrum of 900 °C-aged Cu-LTA(E)PB, exhibit two weak pre-edge peaks around 8980 and 8983 eV, assignable to the $1s \rightarrow 4p$ electronic transition of Cu^+ and Cu^{2+} ions, respectively [8,10], where the higher energy peak is more visible. This indicates that the copper oxide species mainly formed in Cu-LTA(E)PB during hydrothermal aging at 900 °C is CuO. Therefore, the overall characterization results of our study demonstrate that the hydrothermal stability of Cu-LTA catalysts can differ according to the type of raw material sources. Further study is necessary to understand the chemistry behind this observation.

4. Conclusions

The synthesis of high-silica (Si/Al ~ 17) LTA zeolites using economical and safe raw materials compared to the original synthesis recipe in the presence of 12DM3(4MB)I and TMA cations as OSDAs has been investigated. When colloidal silica was used as a Si source, LTA crystallization was found to differ significantly according to its average particle size. The copper-exchanged form of three LTA zeolites, which were synthesized using the same Si and F sources (Ludox HS-40 with an average particle size of 12 nm and NH_4F, respectively) but different Al sources (i.e., aluminum hydroxide, aluminum metal, and pseudoboehmite), when hydrothermally aged at 900 °C showed better activity maintenance for NH_3-SCR than Cu-SSZ-13. However, the Cu-LTA catalyst synthesized using pseudoboehmite as an Al source gave a poor high-temperature activity, unlike the other two catalysts characterized by essentially the same deNO_x activity as that of the original Cu-LTA catalyst at temperatures up to 600 °C, probably due to the formation of inactive CuO_x particles that facilitates the partial structural collapse of the zeolite support. Our study also shows that the hydrothermal stability of Cu-LTA can vary with the type of raw material sources, whereas the extraframework Al species in the zeolite support has little influence on NH_3-SCR. A fluoride-free synthesis route to high-silica LTA zeolites should be developed in order to make Cu-LTA commercially more attractive as an NH_3-SCR catalyst.

Acknowledgements

This work was supported by the National Creative Research Initiative Program (2012R1A3A2048833) through the National Research Foundation of Korea. We thank PAL (Pohang, Korea) for XANES measurement at the 8C beamline (K.-S. Lee). PAL is supported by MSIP and POSTECH.

Appendix A. Supplementary data

Supplementary data associated with this article can be found, in the online version, at https://doi.org/10.1016/j.apcatb.2018.10.042.

References

[1] G. Busca, L. Lietti, G. Ramis, F. Berti, Appl. Catal. B 18 (1998) 1–36.
[2] T.V. Johnson, Int. J. Engine Res. 10 (2009) 275–285.
[3] U.S. Evironmental Protection Agency, Tier 3 Vehicle Emission and Fuel Standards Program, http://www.epa.gov/otaq/tier3.htm (Accessed June 25, 2018).
[4] M. Iwamoto, H. Furukawa, Y. Mine, F. Uemura, S. Mikuriya, S. Kagawa, J. Chem. Soc. Chem. Commun. (1986) 1272–1273.
[5] J.-H. Park, H.J. Park, J.H. Baik, I.-S. Nam, C.-H. Shin, J.-H. Lee, B.K. Cho, S.H. Oh, J. Catal. 240 (2006) 47–57.
[6] S. Brandenberger, O. Kröcher, A. Tissler, R. Althoff, Catal. Rev. 50 (2008) 492–531.
[7] I. Bull, W.-M. Xue, P., Burk, R.S., Boorse, W.M., Jaglowski, G.S., Kroemer, A., Moini, J.A., Patchett, J.C., Dettling, M.T. Caudle, U.S. Patent 7,601,662 B2 (2009).
[8] U. Deka, A. Juhin, E.A. Eilertsen, H. Emerich, M.A. Green, S.T. Korhonen, B.M. Weckhuysen, A.M. Beale, J. Phys. Chem. C 116 (2012) 4809–4818.
[9] Y.J. Kim, H.J. Kwon, I. Heo, I.-S. Nam, B.K. Cho, J.W. Choung, M.-S. Cha, G.K. Yeo, Appl. Catal. B 126 (2012) 9–21.
[10] Y.J. Kim, J.K. Lee, K.M. Min, S.B. Hong, I.-S. Nam, B.K. Cho, J. Catal. 311 (2014) 447–457.
[11] A.M. Beale, F. Gao, I. Lezcano-Gonzalez, C.H.F. Peden, J. Szanyi, Chem. Soc. Rev. 44 (2015) 7371–7405.
[12] K. Chen, K.S. Martirosyan, D. Luss, Chem. Eng. Sci. 66 (2011) 2968–2973.
[13] M. Moliner, C. Franch, E. Palomares, M. Grill, A. Corma, Chem. Commun. 48 (2012) 8264–8266.
[14] R. Martínez-Franco, M. Moliner, A. Corma, J. Catal. 319 (2014) 36–43.
[15] J.H. Lee, Y.J. Kim, T. Ryu, P.S. Kim, C.H. Kim, S.B. Hong, Appl. Catal. B 200 (2017) 428–438.
[16] D.W. Breck, W.G. Eversole, R.M. Milton, T.B. Reed, T.L. Thomas, J. Am. Chem. Soc. 78 (1956) 5963–5972.
[17] B.W. Boal, J.E. Schmidt, M.A. Deimund, M.W. Deem, L.M. Henling, S.K. Brand, S.I. Zones, M.E. Davis, Chem. Mater. 27 (2015) 7774–7779.
[18] D. Jo, T. Ryu, G.T. Park, P.S. Kim, C.H. Kim, I.-S. Nam, S.B. Hong, ACS Catal. 6 (2016) 2443–2447.
[19] T. Ryu, N.H. Ahn, S. Seo, J. Cho, H. Kim, D. Jo, G.T. Park, P.S. Kim, C.H. Kim, E.L. Bruce, P.A. Wright, I.-S. Nam, S.B. Hong, Angew. Chem. Int. Ed. 56 (2017) 3256–3260.
[20] N.H. Ahn, T. Ryu, Y. Kang, H. Kim, J. Shin, I.-S. Nam, S.B. Hong, ACS Catal. 7 (2017) 6781–6785.
[21] J.L. Casci, Microporous Mesoporous Mat. 82 (2005) 217–226.
[22] R.R. Willis, A.I. Benin, Stud. Surf. Sci. Catal. 170 (2007) 242–249.
[23] M. Itakura, I. Goto, A. Takahashi, T. Fujitani, Y. Ide, M. Sadakane, T. Sano, Microporous Mesoporous Mat. 144 (2011) 91–96.
[24] B. Wichterlová, Z. Tvarůžková, Z. Sobalík, P. Sarv, Microporous Mesoporous Mat. 24 (1998) 223–233.
[25] J.A. Lercher, A. Jentys, Stud. Surf. Sci. Catal. 168 (2007) 435–476.
[26] M.C.N.A. de Carvalho, F.B. Passos, M. Schmal, Appl. Catal. A 193 (2000) 265–276.
[27] S.T. Korhonen, D.W. Fickel, R.F. Lobo, B.M. Weckhuysen, A.M. Beale, Chem. Commun. 47 (2011) 800–802.
[28] R. Zhang, N. Liu, Z. Lei, B. Chen, Chem. Rev. 116 (2016) 3658–3721.